Study on the Peripheral Magnetic Leakage and Shielding Measures of Surface-mounted Permanent Magnet Motor*

Fan Rao, Xusheng Wu, Wei Gao and Da Li*

(College of Electrical Engineering, Naval University of Engineering, Wuhan 430033, China)

Abstract: Permanent magnet (PM) motors are widely used in our daily lives. Taking a surface-mounted PM motor as an example, a magnetic circuit model considering the peripheral magnetic flux leakage is established. Maxwell software is used to simulate different loads and thicknesses and the materials of the shielding layers. The magnetic flux leakage around the motor has a sinusoidal distribution in the space. The value of the magnetic flux leakage is inversely proportional to the power of P+1 from the surface of the core. The thicker the shielding layer, the smaller the magnetic leakage. The greater the relative permeability of the shielding layer, the better the shielding effect. The results provide ideas and recommendations for the magnetic flux leakage analysis and the design of non-magnetic or low magnetic motors.

Keywords: Surface-mounted permanent magnet motor, Maxwell software, peripheral magnetic leakage

1 Introduction

In recent years, motor manufacturing and control technology have rapidly developed [1-2]. With the advent of permanent magnet (PM), such as rare-earth metal magnet and neodymium magnet with a high magnetic energy product, small- and medium-power PM motors with excellent performance have been widely used in many fields, including aerospace, military, and agricultural industries [3-5]. In some characteristic fields, such as magnetic field measurement, underwater vehicles, high-precision servo systems, and ships, the external leakage magnetic field of motors may affect the safety concealment of underwater vehicles and ships and may decrease sensor sensitivity [6-8]. Measuring the external magnetic field is a motor fault diagnosis method, which can improve the efficiency of diagnosis [9-10].

Many scholars domestically and abroad have conducted in-depth research on the internal magnetic field leakage theory [11-13] and performed numerical analyses [14-16] of motors. However, few scholars have studied the external magnetic field around motors.

Refs. [17-18] performed a two-dimensional radial and axial magnetic flux leakage simulation analysis on a PM DC motor and measured the magnetic flux leakage intensity of different radii. However, the parameters of the motor are rarely described, and only the simulation model is used to measure the magnetic field.

Refs. [19-20] analyzed the magnetic flux leakage of a PM DC motor under the influence of a shield (No. 10 steel) with different thicknesses (e.g., 0.5 mm, 1 mm, and 1.5 mm). However, compared with Ref. [19], Ref. [20] added an analysis of the transient state of the motor based on static simulation. It concluded that the thicker the shield, the smaller the magnetic flux leakage under a static operation.

Ref. [21] optimized the air gap of the motor shaft and compared the influence of different magnetic isolation measures (magnetic bridge, magnetic sleeve, and non-magnetic shaft) on the air gap magnetic field of the motor.

Ref. [22] presented a standard on a non-magnetic motor but only briefly mentioned that the materials of the motors should be made of non-magnetic materials as far as possible except for the electromagnetic circuit,

Manuscript received April 21, 2021; revised June 20, 2021; accepted October 24, 2021. Date of publication March 31, 2022; date of current version February 13, 2022.
* Corresponding Author, E-mail: depkin@163.com
* Supported by the Youth Program of the National Natural Science Foundation of China (51970970).
Digital Object Identifier: 10.23919/CJEE.2022.000006

and the relative permeability should not be greater than 2.

In this study, the effects of different load conditions of a motor, the thickness of the shielding layer of a surface-mounted PM synchronous motor, and the different shielding layer materials on the magnetic flux leakage distribution around the motor are analyzed.

2 Magnetic circuit model

The external magnetic flux leakage of the motor is very low compared to the main magnetic flux of the motor, and the attenuation is very fast due to the low permeability of air [23]. The external magnetic flux returns to the stator core after passing through the rotor core, PM, working air gap, stator core, and external air. The path is shown in Fig. 1.

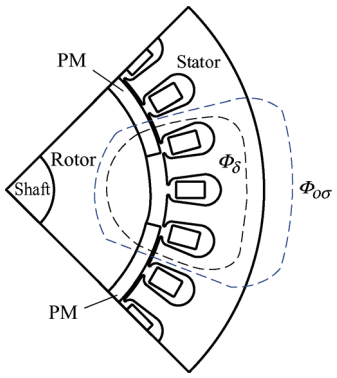

Fig. 1 Magnetic path of the motor

The main part of the magnetic flux provided by the PM passes through the air gap to the stator core and is linked with stator winding, which is called the main magnetic flux Φ_δ, and the corresponding permeance is Λ_δ. A few go directly to the other magnets without passing through the stator core, which is called the internal leakage $\Phi_{i\sigma}$, and the permeance is $\Lambda_{i\sigma}$. Another few passes through the stator core, and the air entering the motor's periphery returns to the stator core, which is called the external leakage magnetic flux $\Phi_{o\sigma}$, and the permeance is $\Lambda_{o\sigma}$ [24]. According to Kirchhoff's law [25] of magnetic circuits, an equivalent magnetic circuit is shown in Fig. 2.

In Fig. 2, F_c is the magnetomotive force of the PM, Λ_0 is the PM internal permeance, Φ_m is the total magnetic flux, F_m is the magnetomotive force provided by each pole PM, and F_a is the armature reaction magnetomotive force.

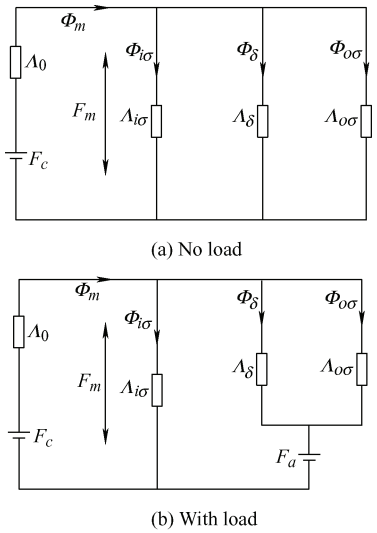

Fig. 2 PM motor equivalent magnetic circuit

By further simplifying the equivalent circuit, the magnetic circuit model is shown in Fig. 3.

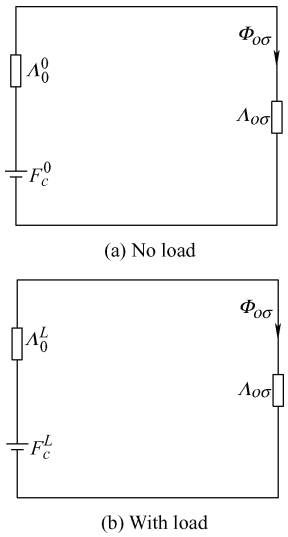

Fig. 3 PM motor equivalent simplified magnetic circuit

The expression without load is

$$F_c^0 = \frac{F_c\Lambda_0}{\Lambda_0+\Lambda_{i\sigma}+\Lambda_\delta} = \frac{F_c\Lambda_0}{\Lambda_0^0}$$

$$\Lambda_0^0 = \Lambda_0+\Lambda_{i\sigma}+\Lambda_\delta$$

The expression with load is

$$F_c^L = \frac{F_c\Lambda_0 - F_a(\Lambda_0+\Lambda_{i\sigma})}{\Lambda_0+\Lambda_{i\sigma}+\Lambda_\delta} = \frac{F_c\Lambda_0+F_a\Lambda_\delta}{\Lambda_0^L} - F_a$$

$$\Lambda_0^L = \Lambda_0+\Lambda_{i\sigma}+\Lambda_\delta$$

The magnitude of the magnetic flux leakage $\Phi_{o\sigma}$ around the motor is related to the equivalent magnetomotive force F_c^0 (F_c^L), equivalent magnetic permeance Λ_0^0 (Λ_0^L), and external leakage permeance

$\Lambda_{o\sigma}$. The equivalent magnetic potential is determined by the performance of the PM, loading condition, main magnetic path, and internal magnetic flux leakage path.

3 Simulation analysis

This simulation selects a surface-mounted PM synchronous motor with eight poles, rated power of 9 kW, and frequency of 60 Hz. The material and motor parameters are shown in Tab. 1.

Tab. 1 Motor parameters

Items	Parameters	Items	Parameters
Stator core material	M36_2G	Rotor outer diameter/mm	176
Rotor core material	M36_2G	Rotor inner diameter/mm	80
Permanent magnet material	XG196_96	Number of pole pairs P	4
Pitch(y)	9	Number of stator lots Z	72
Stator outer diameter/mm	290	Number of conductors per slot (Ws)	66
Stator inner diameter/mm	180	Number of turns in series per phase N	792

The motor is composed of 72 slots and 8 poles and adopts a 60° phase band arrangement. Taking the electromotive force under a pair of poles (18 slots) as an example, the star figure of the slot electromotive force is shown in Fig. 4. Fig. 5 shows the motor model built using Maxwell finite element software.

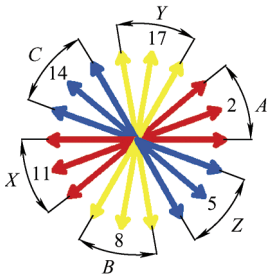

Fig. 4 Slot electromotive star map (a pair of pole)

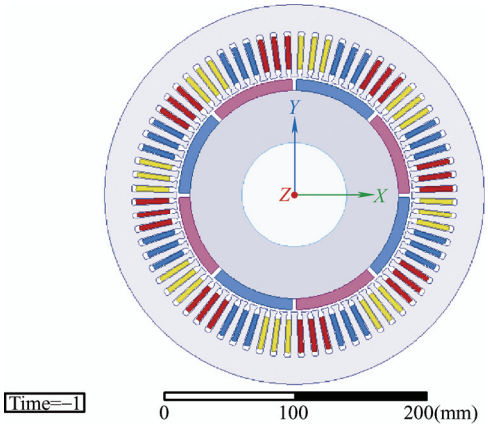

Fig. 5 Maxwell motor model

The direction and distribution of the magnetic field lines are shown in Fig. 6, where the motor is in the rated state (the AC winding voltage is 234 V, and the rotor speed is 900 r/min) and the startup process of the motor is ignored.

Fig. 6b clearly shows that the value and direction of the magnetic flux leakage are related to the position of the motor, its external magnetic field is few, and most of magnetic flux passes through the stator core and rotor to form a loop.

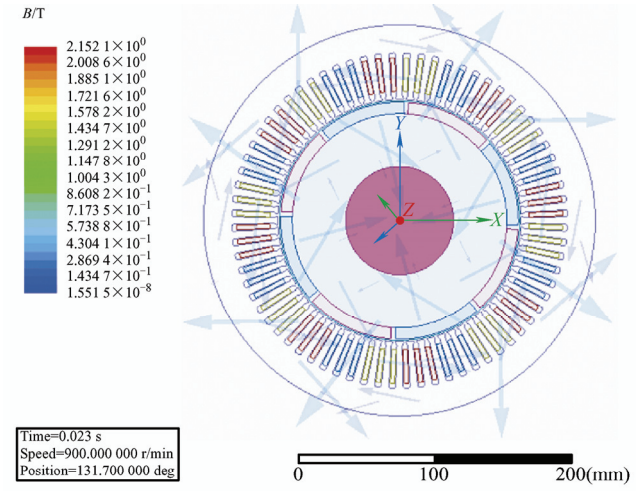

(a) Magnetic induction intensity

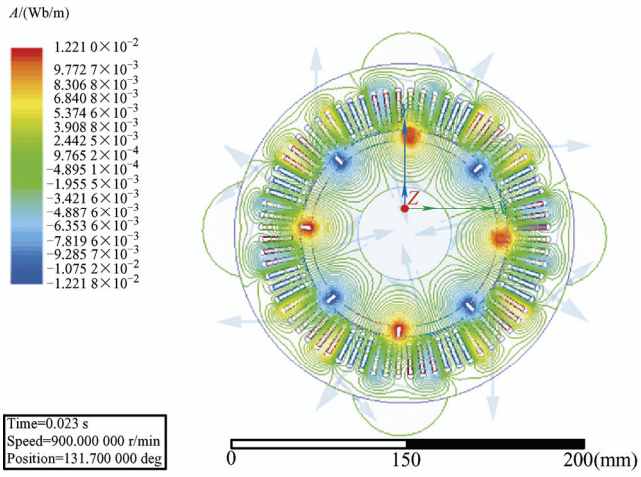

(b) Magnetic field lines

Fig. 6 Simulation results

3.1 Different loading conditions

When the motor has a rated load, the direction and value of its magnetic induction strength greatly vary depending on the spatial position. Different measuring circles are set around the motor, and its magnetic induction intensity is shown in Fig. 7.

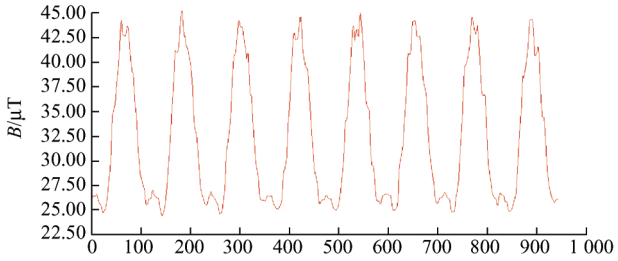

(a) Distance=5 mm

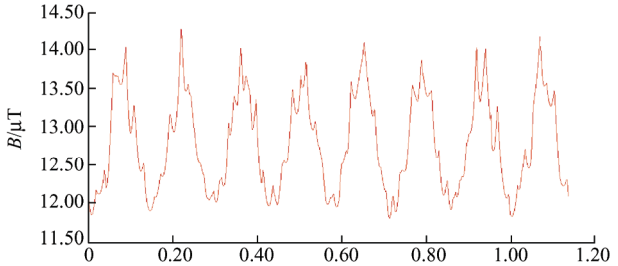

(b) Distance=35 mm

Fig. 7 Peripheral magnetic leakage of the motor at different distances from the core

On the same measurement radius, the magnetic induction intensity changes approximately with a sinusoidal distribution, but the change is not large. Its value greatly varies at different measurement distances. For example, if the distance is 5 mm, B≈44 μT, whereas if the distance is 35 mm, B≈14 μT. The average of the maximum magnetic flux values at different measurement points is shown in Tab. 2.

Tab. 2 Maximum magnetic induction at different measuring distances at full load

Distance/mm	5	15	35	95	200	400	600	800
B/nT	44 000	27 600	13 850	3 090	497	50.3	10.65	3.35

Tab. 2 shows that the larger the distance, the faster the decay of the magnetic induction intensity, and B presents a nonlinear distribution. When the distance ⩾600 mm, the magnetic flux is less than 10 nT.

To compare different load conditions, the same measurement position is set when the motor has no load, and the maximum average value is taken. The magnetic flux leakage value of the motor in the two load conditions is shown in Fig. 8.

From the perspective of the results, the magnetic flux leakage shows a nonlinear distribution. Fitting the curve in Fig. 8, the following equations can be obtained

Full load

$$B(r)=3.1\times10^{15}\times r^{-5}=3.1\times10^{15}\times(d+145)^{-5}$$

No load

$$B(r)=1.61\times10^{16}\times r^{-5}=1.61\times10^{16}\times(d+145)^{-5}$$

where r is the distance from the measuring point to the center of the motor and d is the distance from measuring point to the surface of the motor. B is inversely proportional to the 5th (4(number of pole pairs)+1) power of r or d. The magnetic flux leakage at the no-load condition is obviously larger than that at the full-load condition, at approximately 1 order of magnitude.

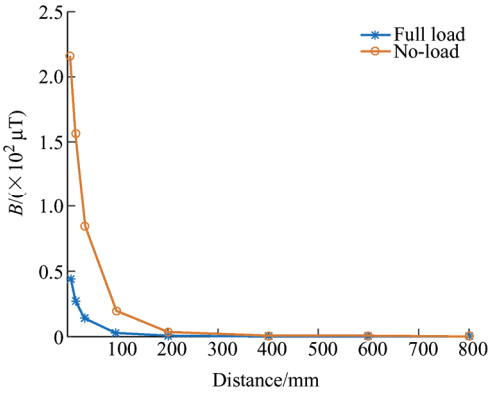

Fig. 8 Magnetic flux leakage around the motor under different load conditions

3.2 Shield of different thicknesses

To reduce the external magnetic leakage, the use of a shielding layer is a very effective measure. The Maxwell motor shielding layer model and its magnetic line distribution are shown in Fig. 9.

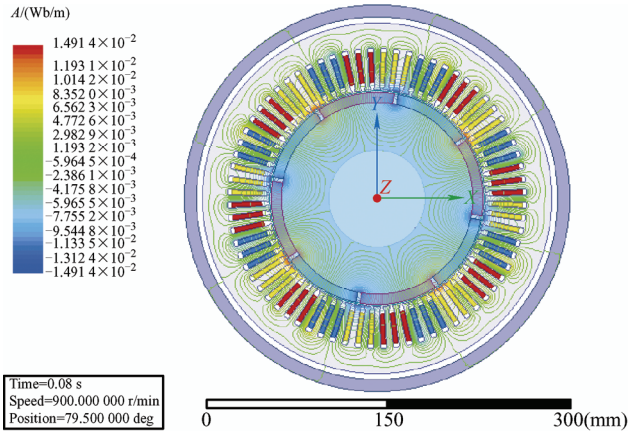

Fig. 9 Motor model with the shielding layer

At the same shielding layer material (D21-50) and different thicknesses, the external magnetic flux leakage is shown in Fig. 10.

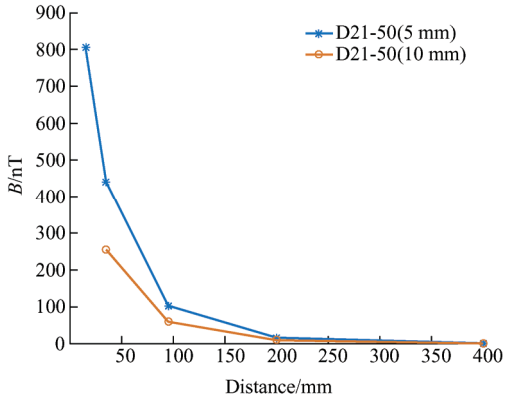

Fig. 10 Magnetic flux leakage of the motor peripheral with different thicknesses of the shielding layer

When the materials of the shielding layer are the same, the change trend of the magnetic flux leakage around the motor is the same. The thicker the shielding layer, the better the shielding effect. In the example, the magnetic leakage of the 10 mm shielding layer is 58% of that of the 5 mm shielding layer, which is approximately 1.72 times better.

3.3 Shield of different materials

The material of the shielding layer also has a large effect on the shielding effect. To compare the magnetic flux leakage of different materials, two shielding materials with the same thickness (DW310-35 and D21-50) are selected for the simulation analysis. The magnetization curves of the two materials are shown in Fig. 11.

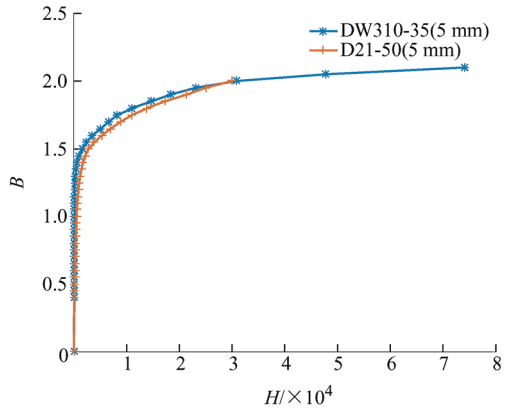

Fig. 11 Magnetization curves of different materials

By simulating the shielding layers of the two materials, the magnetic flux density is measured and the maximum values are averaged. The distribution of the magnetic flux leakage with distance for the two materials is measured and shown in Fig. 12.

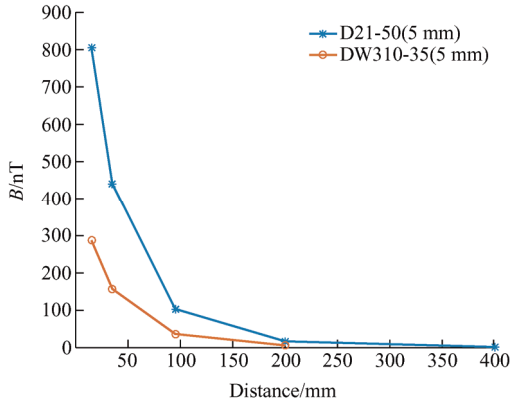

Fig. 12 Magnetism leakage with different materials

From the simulation results, the greater the relative permeability, the better the shielding effect. This is because with a larger one, the relatively magnetic permeability makes it easier to conduct a magnetic flux, and the magnetic lines of force can easily pass through, so most of the magnetic flux will return to the stator core from the path with a small resistance. The leakage flux of DW310-35 material is approximately 36% of that of the D21-50 material.

3.4 Comparison of various situations

Fig. 13 shows the distribution of the magnetic induction intensity at different distances at full load without shielding, D21-50 (5 mm) shielding, D21-50 (10 mm) shielding, and DW310-35 (5 mm) shielding at various distances.

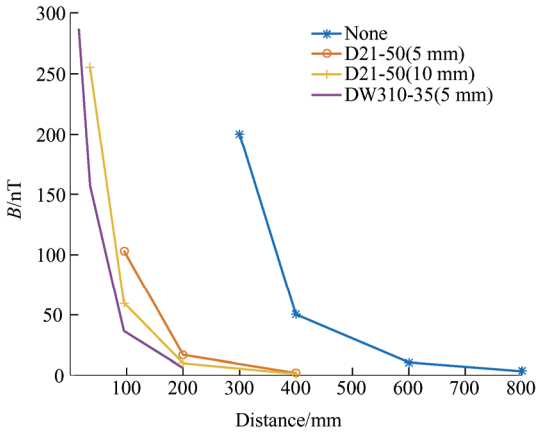

Fig. 13 Magnetism leakage of under different conditions

Whether there are shielding measures, the magnetic leakage attenuation around the motor is a nonlinear distribution. If there is a shield, part of the magnetic flux leakage around the motor will return to the stator core through the shielding barrier. The thicker the same shielding material, the better the shielding effect.

The larger the relative permeability of the same thickness of the material, the better the shielding effect. However, DW315-35(5 mm) leakage is approximately 61% of D21-50(10 mm). Therefore, when selecting a shielding layer, it is preferred to use a large relatively magnetic permeability, which can not only reduce the thickness of the shielding layer to achieve the same shielding effect but also increase the power density of the motor.

4 Conclusions

The magnetic flux leakage around the motor has a sinusoidal distribution in the space. The value of magnetic leakage is inversely proportional to the power of P+1 from the surface of the core (P is the number of pole pairs). The thicker the shielding layer, the smaller the magnetic leakage. The greater the relative permeability of the shielding layer, the better the shielding effect. Selecting a shielding material with a better magnetic permeability can not only achieve a better shielding effect but also greatly reduce the thickness of the shielding layer, which is conducive to improving the power density of the motor.

References

[1] R Y Tang. Theory and design of modern permanent magnet motor. Beijing: China Machine Press, 2016.

[2] L F Geng, Y Z Wu. Development trend of modern permanent magnet motor. *Journal of Shenyang University of Technology*, 1995(1): 25-28.

[3] A Higuchi, S Hirosawa. Sintered Nd-Fe-B permanent magnets. *IEEE Transactions on Magnetics*, 1989, 25(5): 3555-3560.

[4] B Li. Analysis and reducing techniques review of torque ripple for permanent magnet brushless motor. *Electric Machines & Control Application*, 2011, 38(4): 6-12.

[5] E A Lomonova, E Kazmin, Y Tang, et al. In-wheel PM motor: Compromise between high power density and extended speed capability. *Compel International Journal for Computation & Mathematics in Electrical & Electronic Engineering*, 2009, 30(1): 98-116.

[6] Y F Wang. Research on magnetic interference compensation technology for airborne geomagnetic measurement. Wuhan: Huazhong University of Science and Technology, 2012.

[7] X J Liu. Research on magnetic interference compensation algorithm based on underwater robot. Harbin: Harbin Institute of Technology, 2018.

[8] T Lubin, S Mezani, A Rezzoug. Exact analytical method for magnetic field computation in the air gap of cylindrical electrical machines considering slotting effects. *IEEE Transactions on Magnetics*, 2010, 46(4): 1092-1099.

[9] R Romary, D Roger, J F Brudny. Analytical computation of an AC machine external magnetic field. *European Physical Journal Applied Physics*, 2009, 47(3): 1-6.

[10] R Romary, S Jelassi, F Brudny. Stator-interlaminar-fault detection using an external-flux-density sensor. *IEEE Transactions on Industrial Electronics*, 2010, 57(1): 237-243.

[11] J K Lee. A study on analysis of synchronous reluctance motor considering axial flux leakage through end plate. *IEEE Transactions on Magnetics*, 2019: 1-4.

[12] Y Feng, F Li, S Huang, et al. Variable-flux outer-rotor permanent magnet synchronous motor for in-wheel direct-drive applications. *Chinese Journal of Electrical Engineering*, 2018, 4(1): 28-35.

[13] X T Zhang, P Fu, Y Ma, et al. No-load iron loss model for a fractional-slot surface-mounted permanent magnet motor based on magnetic field analytical calculation. *Chinese Journal of Electrical Engineering*, 2018, 4(4): 71-79.

[14] J W Jung, M S Lim, J P Hong, et al. Characteristics analysis of SPMSM using 2-D finite-element analysis considering axial leakage flux. *IEEE Transactions on Magnetics*, 2017, 54(3): 1-4.

[15] M Dai, A Keyhani, T Sebastian. Torque ripple analysis of a PM brushless DC motor using finite element method. *IEEE Transactions on Energy Conversion*, 2004, 19(1): 40-45.

[16] Y Kawase, T Yamaguchi. Analysis of cogging torque of permanent magnet motor by 3-D finite element method. *IEEE Trans. Magn*., 1995, 31(3): 2044-2047.

[17] W Li, B W Song, Y L Hu. Numerical analysis of magnetic leakage field of permanent magnet DC motor for underwater vehicle. *Machinery & Electronics*, 2011(3): 33-35, 38.

[18] F P Li, Y L Hu, J B Dong. Simulation analysis of magnetic flux leakage of permanent magnet DC motor based on magnet. *Small & Special Machines*, 2010, 38(4): 27-29.

[19] W Li, B W Song, Y L Hu. Magnetic flux leakage simulation of permanent magnet DC motor. *Small & Special Machines*, 2010, 38(9): 16-18.

[20] J M Li, Y L Hu. Analysis of the influence of shield on the magnetic field of permanent magnet DC motor. *Small & Special Machines*, 2011, 38(8): 19-22.

[21] C Y Sun, M J Liu, Y L Luo, et al. Shaft leakage analysis of different rotor structures of tangential permanent

magnet synchronous motor. *Small & Special Machines*, 2010(2): 27-29.

[22] Naval Sea Systems Command, Department of the Navy. MIL DTL 17060-2016 motors, alternating current, integral-horsepower, shipboard use. Washington: Military and Government Specs & Standards, 2016.

[23] S B Liao. Ferromagnetism. Beijing: Science Press, 1988.

[24] X H Wang. Permanent magnet motor. Beijing: China Electric Power Press, 2007.

[25] A E Fitzgerald, C K Jr, S D Umans. Electric machinery. NewYork: McGraw-Hill, 2005.

Fan Rao was born in Sichuan province, China. He is currently working toward the M.Eng. degree in Electrical Engineering School of Naval University of Engineering, Wuhan, China. And his research interests focus on electrical machine, modeling, simulation, PM machines.

Xusheng Wu was born in Jinhua, Zhejiang Province, in 1976. He received his Ph.D. in Electrical Engineering from Naval University of Engineering in 2003 and worked in the post-doctoral research station of Electrical Engineering of Wuhan University from 2004 to 2007. His research interests include power integration technology, wireless power transmission.

Mr. Wu's doctoral thesis was awarded the excellent doctoral thesis of Hubei Province in 2004, and he won the first prize of National Science and Technology Progress in 2010.

Wei Gao was born in Zibo, Shandong Province, in 1980. He received his Ph.D. in Electrical Engineering from Naval University of Engineering in 2011 and in the post-doctoral research station of the 28th Research Institute of Electronic Technology Group. His research interests include wireless power transmission, electrical machinery and appliances.

Mr. Gao has published 45 academic papers and a monograph, applied for 7 invention patents, supported or participated in 26 scientific research projects as the main completer. Mr. Gao is a senior member of China Electrical Technology Society and China Power Supply Society.

Da Li was born in Wuhan, Hubei Province, in 1994. He is currently studying for his Ph.D. in Electrical Engineering at the School of Electrical Engineering, Naval University of Engineering. His research interests include wireless power transmission, RFID technology and its application, antenna design and test.